The Astrophysical Journal, 770:11 (14pp), 2013 June 10 doi:10.1088/0004-637X/770/1/11

SOLAR ENERGETIC PARTICLE MODULATIONS ASSOCIATED WITH COHERENT MAGNETIC STRUCTURES

L. Trenchi[1], R. Bruno[1], D. Telloni[2], R. D'amicis[1], M. F. Marcucci[1], T. H. Zurbuchen[3], and M. Weberg[3]
[1] INAF-Istituto di Astrofisica e Planetologia Spaziali, Via del fosso del Cavaliere 100, 00133 Rome, Italy; lorenzo.trenchi@iaps.inaf.it
[2] INAF, Astronomical Observatory of Torino, Via Osservatorio 20, 10025 Pino Torinese, Italy
[3] Department of Atmospheric, Oceanic, and Space Sciences, University of Michigan, Ann Arbor, MI, USA
Received 2013 February 5; accepted 2013 April 16; published 2013 May 20

ABSTRACT

In situ observations of solar energetic particles (SEPs) often show rapid variations of their intensity profile, affecting all energies simultaneously, without time dispersion. A previously proposed interpretation suggests that these modulations are directly related to the presence of magnetic structures with a different magnetic topology. However, no compelling evidence of local changes in magnetic field or in plasma parameters during SEP modulations has been reported. In this paper, we performed a detailed analysis of SEP events and we found several signatures in the local magnetic field and/or plasma parameters associated with SEP modulations. The study of magnetic helicity allowed us to identify magnetic boundaries, associated with variations of plasma parameters, which are thought to represent the borders between adjacent magnetic flux tubes. It is found that SEP dispersionless modulations are generally associated with such magnetic boundaries. Consequently, we support the idea that SEP modulations are observed when the spacecraft passes through magnetic flux tubes, filled or devoid of SEPs, which are alternatively connected and not connected with the flare site. In other cases, we found SEP dropouts associated with large-scale magnetic holes. A possible generation mechanism suggests that these holes are formed in the high solar corona as a consequence of magnetic reconnection. This reconnection process modifies the magnetic field topology, and therefore, these holes can be magnetically isolated from the surrounding plasma and could also explain their association with SEP dropouts.

Key words: interplanetary medium – magnetic fields – Sun: flares – Sun: particle emission – turbulence

Online-only material: color figures

1. INTRODUCTION

Particle acceleration is a common phenomenon in the heliosphere, which can produce energetic particles ranging from tens of keV to GeV. The solar energetic particles (SEPs) can be generated either by solar flares or by shocks driven by coronal mass ejection (CME) through processes such as diffusive shock acceleration, also referred to as Fermi I acceleration. SEPs from solar flares can be distinguished from those accelerated by interplanetary shocks because of the enhancement of heavier ion abundance with respect to SEPs from interplanetary shocks (Reames 1999). Moreover, since the duration of the acceleration process at the impulsive solar flares is much shorter than the propagation time to 1 AU (Miller & Vinas 1993), we can observe a measurable velocity dispersion in the distribution of the particle velocities in an energy versus time spectrum. Very often, in situ observations of the low-energy (up to a few MeV) intensity profile of SEPs from impulsive solar flares have shown dropouts, limited by very sharp boundaries, affecting all energies at the same time (dispersionless phenomenon; Chollet & Giacalone 2008). These clear particle voids would then suggest that their origin must be searched not at the originating site but rather during their propagation along the background interplanetary magnetic field. Although this conclusion is rather unanimous within the scientific community, the physical mechanism at the basis of this phenomenon is rather unclear.

Mazur et al. (2000) suggested that these dropouts are related to magnetic flux tubes originating at the Sun and extending in the heliosphere to 1 AU and beyond. In the model proposed by Mazur et al. (2000), during the advection, the footpoint motion has the effect that adjacent flux tubes at 1 AU can be widely separated at the Sun and, conversely, that adjacent flux tubes at the Sun may be separated at 1 AU. If the spacecraft—at the moment when the SEP phenomenon is observed—passes through magnetic flux tubes that are alternatively connected and not connected with the flare site, particle dropouts will be observed. Moreover, Gosling et al. (2004) also reported dispersionless modulations of suprathermal electron fluxes associated with modulation of SEPs. The observed association of these phenomena demonstrates that the modulations in both particle species have a common origin that could be due to changes in magnetic connection with the corona at the flare site.

Giacalone et al. (2000) provided the first description of dropouts based on a computational model, adopting the idea of a random walk of interplanetary magnetic field lines during solar wind expansion. They found that modulations of the SEP fluxes, associated with remarkably steep spatial gradients very similar to what has been observed at 1 AU, are expected when the source region that impulsively releases the energetic particles is small compared with the field correlation scale. Conversely, no dropouts are expected when the injection region is rather large, i.e., several magnetic field correlation scales. Other authors addressed the specific role of turbulence in SEP modulation attributing a different role to SLAB and two-dimensional (2D) components (Matthaeus et al. 1990). Following Ruffolo et al. (2003), as the wind expands, magnetic field lines remain trapped within regions dominated by 2D turbulence forming a sort of filamentary structure in 3D space, while in regions dominated by slab turbulence they are largely diffused. It follows that a spacecraft crossing alternating regions of 2D and slab magnetic turbulence populated with SEPs from a localized source region near the Sun would observe the typical SEP dropouts. However,

Pommois et al. (2005) found that both the spatial structure of particle distribution and transport properties, parallel and perpendicular to the background field, strongly depend on the turbulence anisotropy. In particular, results of their numerical model showed that whenever the perpendicular correlation length is larger than the parallel correlation length (i.e., when slab turbulence dominates 2D turbulence), SEP concentrations and dropouts should be observed. These results then do not seem to agree with the model suggested by Ruffolo et al. (2003) and motivated us to more deeply investigate the local topology of magnetic field lines and the variation of plasma parameters, using available in situ observations, in order to test which of these models better explain the observed SEP modulations.

In this paper we will test one aspect of the problem, i.e., the possibility that SEP dropouts are directly connected to the presence of magnetic flux tubes connected or disconnected with the energetic particle source region, leaving arguments more closely related to the turbulence character of the fluctuations to future analyses. To do so, we will analyze in situ observations of solar wind parameters during SEP dropout events aiming to unravel the presence of magnetic flux tubes. As a matter of fact, interplanetary magnetic flux tubes were identified in the solar wind using a wavelet technique by studying magnetic field intermittence (Bruno et al. 2001). These authors suggested that the discontinuities in magnetic field intensity associated with arc-like field rotations and with variations of plasma pressure and velocity might be the borders between two adjacent magnetic flux tubes. Later on, Borovsky (2008) performed a robust statistical study on interplanetary magnetic field discontinuities using seven years of measurements with the *ACE* spacecraft at 1 AU. He was able to detect a large number of flux tubes whose walls showed large changes in the magnetic field direction and vector flow velocity, and significant changes of other plasma parameters.

Our study will be a natural succession of this earlier work, but will add two complementary aspects: a detailed analysis of magnetic helicity and the inclusion of solar wind compositional data. The first part of the analysis performed in this paper will be based on the study of the local magnetic field topology by means of magnetic helicity in order to identify the borders of different flux tubes. This will be followed by a detailed analysis of plasma parameters to corroborate magnetic findings. We will show how the analyzed dropout events are related to the presence of interplanetary flux tubes that connected or disconnected with the flare region.

2. DATA ANALYSIS

In this paper, we will consider several SEP events measured by *ACE* or *WIND* between 1998 and 2002. The data of energetic ions, in the energy range from 0.02 to 2 MeV nucleon^{-1}, were obtained from Ultra Low Energy Spectrometer (Mason et al. 1998) on board *ACE* and from SupraThermal Energetic Particle System (von Rosenvinge et al. 1995) on board *WIND*. Magnetic field and plasma data were obtained from MAG (Smith et al. 1998) and SWEPAM (McComas et al. 1998) on board *ACE* and from *WIND* Magnetic Field Investigation (Lepping et al. 1995) and 3D Plasma Analyzer (Lin et al. 1995) on board *WIND*, respectively. Moreover, for one SEP event the plasma heavy-ion composition data measured by SWICS (Gloeckler et al. 1998) on board *ACE* have been studied. The GSE reference system is used. The first tool that we used to unravel the presence of magnetic flux tubes exploited the fact that, passing from one tube to the next one, the local mean magnetic field experiences a remarkable directional rotation (Bruno et al. 2001; Borovsky 2008; Li 2008). These directional rotations enhance the magnetic helicity value of the local field and an appropriate magnetic helicity evaluation can be used to spot arc-like coherent structures. The magnetic helicity is a physical descriptor of magnetic field topology which measures the twist of magnetic field lines. It is defined as

$$H_m = \int \mathbf{A} \cdot \mathbf{B}\, d^3\mathbf{x}, \tag{1}$$

where **B** is the magnetic field vector and **A** is the vector potential. With measurements from a single spacecraft, it is not possible to evaluate the magnetic helicity without spatial information on the properties of the magnetic field. However, adopting Taylor's hypothesis and being in a situation of collinear measurements from one single spacecraft, it is possible to evaluate a surrogate of this quantity called reduced magnetic helicity (Matthaeus & Goldstein 1982). These authors provided the following simplified form to compute the reduced H_m for collinear measurements:

$$H_m^r(k) = \frac{2Im[Y^*(k) \cdot Z(k)]}{k}, \tag{2}$$

where Y and Z are the Fourier coefficients of the components of the magnetic field B_y and B_z (both perpendicular to the sampling direction x along the radial direction), respectively, and * indicates the complex conjugate. The first measurements of this reduced quantity in the solar wind (Matthaeus & Goldstein 1982; Bruno & Dobrowolny 1986) showed that $H_m(k)$ continuously reverses its sign moving across the low-frequency spectral range. It is clear that if we aim to spot localized helicity structures we have to separate the time domain from the spectral domain by the use of wavelet transforms (i.e., Bruno et al. 2008; He et al. 2011; Podesta & Gary 2011). Using the wavelet transform (Torrence & Compo 1998), Equation (2) can be rewritten as

$$H_m^r(k,t) = \frac{2Im[W_y^*(k,t) \cdot W_z(k,t)]}{k}, \tag{3}$$

where $W_y(k,t)$ and $W_z(k,t)$ are complex wavelet transforms of B_y and B_z components of the magnetic field and superscript * indicates the complex conjugate. The adopted mother wavelet generally depends on the aim of the study. In our specific case, Paul and Morlet wavelets are the ideal candidates since they are complex and yield complex wavelet transforms, which are needed to evaluate magnetic helicity. The analysis that follows has been performed using Paul as the mother wavelet. As a matter of fact, although the Morlet wavelet basis has sharper scale identification capabilities, the Paul wavelet basis shows a better time resolution and has a smaller Cone Of Influence (hereafter indicated as COI) and thus it is less affected by edge effects. For this reason we chose to use the Paul basis throughout the analysis shown in this paper. This new technique, recently adopted to localize small-scale magnetic flux ropes (Telloni et al. 2012), allows us to identify the large field rotations that could be related to flux tube boundaries. Successively, we will use plasma parameters to highlight possible differences existing between different solar wind regions as identified by H_m analysis.

2.1. 1999 April 21–22 Event

The first SEP event that we illustrate (panels (a) and (b) in Figure 1) is the one measured by *ACE* during 1999 April 21–22

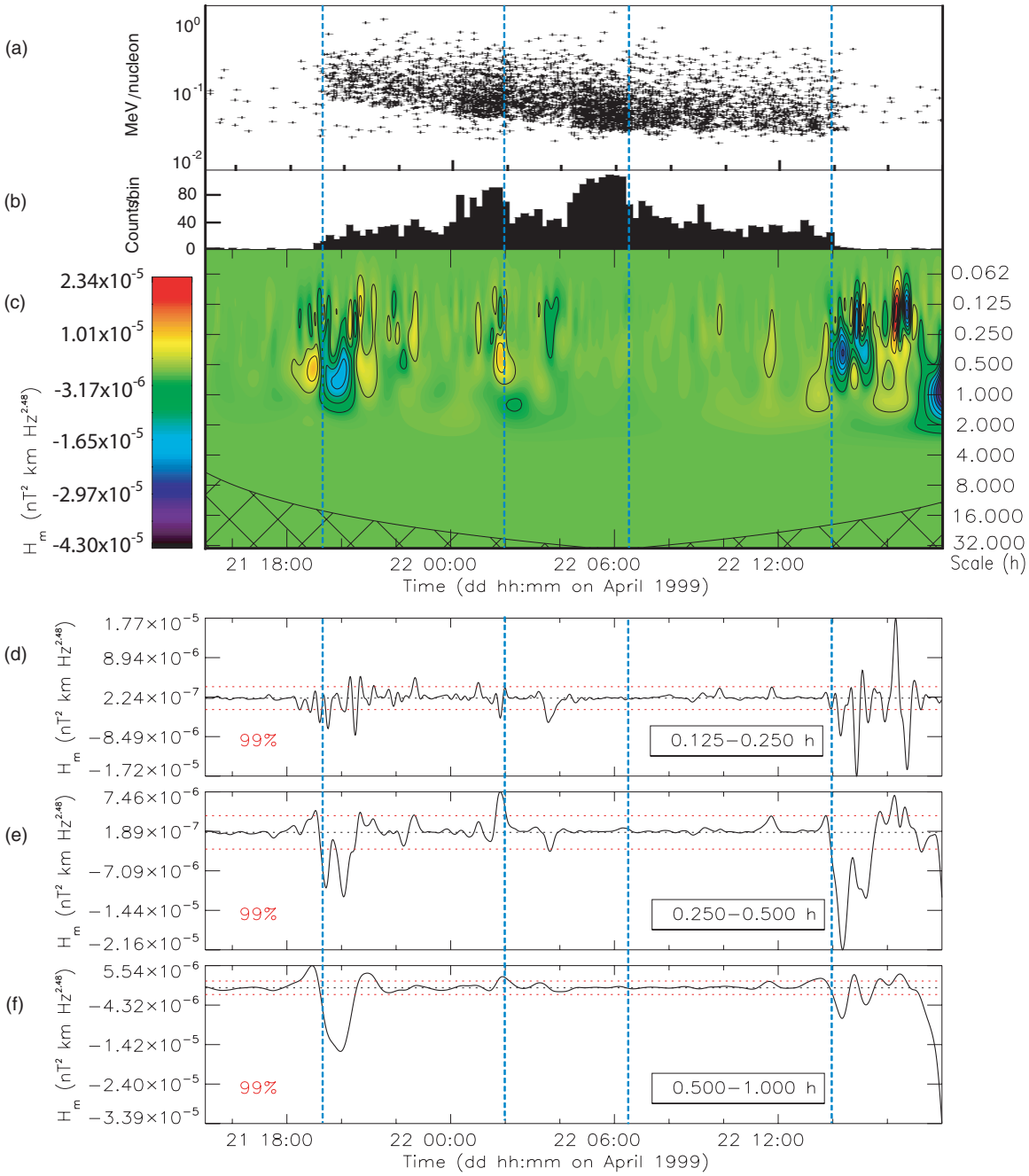

Figure 1. Combined energetic ions (adapted from Gosling et al. 2004) and magnetic helicity analysis for the 1999 April 21–22 SEP event. (a) The energy of heavy ions (in units of MeV nucleon^{-1}) vs. their arrival time. (b) The ion counts, integrated over all energies, vs. time in about 14 minute bin. In the subsequent panels, the results of magnetic helicity analysis are shown. (c) The compensated magnetic helicity values, obtained by multiplying $H_m^r(k, t)$ by $f^{2.48}$, are reported with the color scale, where the right axis indicates the timescales in hours and the cross-hatched area marks the COI where edge effects become important. (d)–(f) The significance level of the average H_m value, within the frequency range indicated in each panel, with respect to the significance level of 99% shown by the dotted red lines.

(A color version of this figure is available in the online journal.)

(Mazur et al. 2000; Gosling et al. 2004). The spectrogram in panel (a) shows the energy (in units of MeV nucleon^{-1}) of energetic heavy ions versus their arrival time while in panel (b) the energetic ion counts, integrated over all energies, versus time, in about 14 minute bin, are plotted (adapted from Gosling et al. 2004). The SEP event starts approximately at 19:12 of April 21 with the arrival of first particles in the energy range 0.1–0.5 MeV nucleon^{-1} and finishes at 14:00 of April 22 when the last particles in the energy range 0.03–0.2 MeV nucleon^{-1} are detected (panel (a), blue dotted lines). Both the onset and the end of this SEP event are dispersionless and can be easily identified because of the very low level of particle background, <5 particles bin^{-1}. During this event the SEP counts do not decrease to the background level and the SEPs are continuously observed. However, two peaks of the SEP counts are observed around 01:30 and 05:00 of April 22 where the counts rise up to 80 particles bin^{-1} and then sharply decrease (blue dotted lines). The clear dispersion relation observed within this 19 hr SEP event suggests that these particles were impulsively accelerated at the Sun. The subsequent panels in Figure 1 show the results

of magnetic helicity analysis in the form of the so-called scalogram. In this 3D histogram, the time is on the horizontal axis, scales (in hours) on the vertical axis, and magnetic helicity value is given by the color, as shown by the color scale located on the left-hand side of the panel. In order to highlight possible magnetic helicity signatures at all scales (Telloni et al. 2012), spectral values were compensated multiplying them by f^{α}, with f being the corresponding frequency and α the spectral index obtained from the Fourier spectrum of magnetic helicity. In order to estimate α, positive and negative values of H_m were put together in a single power density spectrum. The advantage of doing so is that magnetic helicity signatures contained in the smallest scales can also be revealed and plotted in the same scalogram together with the largest scales.

In this particular case the spectral index was -2.48 and helicity values were multiplied by $f^{2.48}$. This particular value of α is not far from $-8/3$ expected for H_m spectral index for developed turbulence literature (Matthaeus & Goldstein 1982; Bruno & Dobrowolny 1986).

Compensated magnetic helicity values obtained by multiplying $H_m^r(k, t)$ by $f^{2.48}$ are reported with the color scale in panel (c), where the right axis indicates the timescales in hours. The cross-hatched area shown in the same panel corresponds to the COI, which indicates the regions in which edge effects, due to finite-length time series, become important. Features below the continuous curved line (i.e., at larger scales) are not fully reliable. Panels (d)–(f) show the significance level of H_m values for three different frequency bands between 7.5 minutes and 1 hr.

We chose these limits based on the findings by Bruno et al. (2001). These authors found that the average elapsed time between consecutive intermittent events of magnetic field and wind velocity was around 30 minutes and they interpreted these events as the crossing of the border between adjacent flux tubes. Since the main goal of this paper is to identify local flux tubes that might cause SEP modulation, we filtered out smaller and larger scales from the original data. A significance level of 99% is shown by the dotted red lines in each of the three panels while the continuous black line shows the average H_m value within the frequency range indicated in each panel. A white noise signal has been used to establish a null hypothesis to evaluate the significance of a peak of H_m time series obtained by averaging over all the discrete frequencies within the frequency range of interest. The significance level is expected to follow a χ^2 distribution with n degrees of freedom, where n is the number of scales (frequencies) averaged in the process. If one peak is above the 99% confidence level it means that there is only a 1% probability that we obtained this result by mere chance. A detailed description of the significance analysis is reported in the Appendix.

The more evident helicity structures, detected around 20:00 of April 21 and around 15:00 of April 22, are significant at all the three scales examined according to the significance level of 99%. It can be noted that these helicity structures roughly match the dispersionless onset and the dispersionless end of this SEP event. These observations may suggest that the region where SEPs are detected has a different magnetic topology with respect to the surrounding plasma. Moreover, the small helicity structure observed at 02:00 of April 22 seems to be associated with the sharp decrease of SEP counts.

Afterward, we analyzed plasma parameters observed during the same SEP event in detail in order to find signatures that could corroborate previous findings based only on magnetic helicity analysis. These observations are shown in Figure 2 where, for the reader's convenience, the top two panels are the same as shown in Figure 1. In panels (c)–(g), plasma and magnetic field parameters are reported: the ratio between plasma and magnetic pressures β and the α to proton density ratio (panel (c)), kinetic, magnetic, and total pressures (panel (d)), plasma density and temperature (panel (e)), magnetic field magnitude and plasma speed (panel (f)), and, finally, the polar angles of the magnetic field vector defined as $\varphi = \tan^{-1}(B_Y/B_X)$, $\theta = \tan^{-1}(B_Z/(B_X^2 + B_Y^2)^{0.5})$ in the range $[-180^\circ, +180^\circ]$ and $[-90^\circ, +90^\circ]$, respectively (panel (g)).

It is important to mention that during 1999 April 21–22 *ACE* is probably observing a CME and the SEPs are propagating within the CME's magnetic structure. In fact, during this SEP event the typical characteristics of CMEs (Neugebauer & Goldstein 1997; Zurbuchen & Richardson 2006) such as high α/proton density ratio, low plasma β, a smooth magnetic field rotation, and counterstreaming electrons (Gosling et al. 2004) are observed. The spacecraft most likely enters the CME several hours before the onset of the SEP event, at 09:00 of April 21, when the first counterstreaming electrons are detected (Gosling et al. 2004) and the energetic particle background decreases (not shown). However, the SEP modulations correspond to sharp variations of plasma and magnetic field parameters associated with the observed helicity structures, which could identify magnetic boundaries internal to this CME: at 19:30 of April 21 the increase of α/proton density ratio and of plasma temperature and the decrease of plasma number density match the dispersionless onset of SEP event; similarly, the modulations of the SEP counts at 02:00 and 06:30 of April 22 (blue dotted lines) seem to be associated with variations of density and temperature of plasma and with variations of α/proton density ratio. The dispersionless end of SEP event roughly corresponds with the exit from the CME, corresponding to an increase in plasma density and temperature and a decrease in magnetic field magnitude. These observations suggest that the magnetic boundaries associated with the dispersionless margins of this SEP event identify a magnetic flux tube, internal to the CME, where SEPs are propagating.

2.2. 1998 April 11–12 Event

The second SEP event that we discuss here (panels (a) and (b) in Figure 3) is the one measured by *ACE* in the course of 1998 April 11–12 (Mazur et al. 2000; Gosling et al. 2004). Panels (a) and (b) have the same format as those in Figures 1 and 2, but here only the data relative to energetic heavy ions, from He to Fe, are plotted (adapted from Gosling et al. 2004). This SEP event starts at about 20:00 on April 11 with the arrival of ions with energy of about 2 MeV, ends at 19:00 on April 12, and is superposed with a 30 particles bin^{-1} background of particles of about 0.1 MeV nucleon^{-1} coming from a gradual solar event that began on April 4 (Gosling et al. 2004). The main feature of this event is the long duration interruption of the SEP, observed between 01:30 and 08:00 on April 12, where no SEPs are detected and the counts decrease to the background level (region 2). The SEP event is therefore divided into two blocks: from 20:00 on April 11 to 01:30 on April 12 with higher energy SEPs (region 1) and from 08:00 to 19:00 on April 12 with lower energy SEP particles (region 3). The clear dispersion relation of the SEP in agreement between regions 1 and 3 and the presence of SEP heavy ions (Gosling et al. 2004) demonstrates that these SEPs were impulsively accelerated at the Sun. It can be noted that the SEP counts differ substantially from region 1

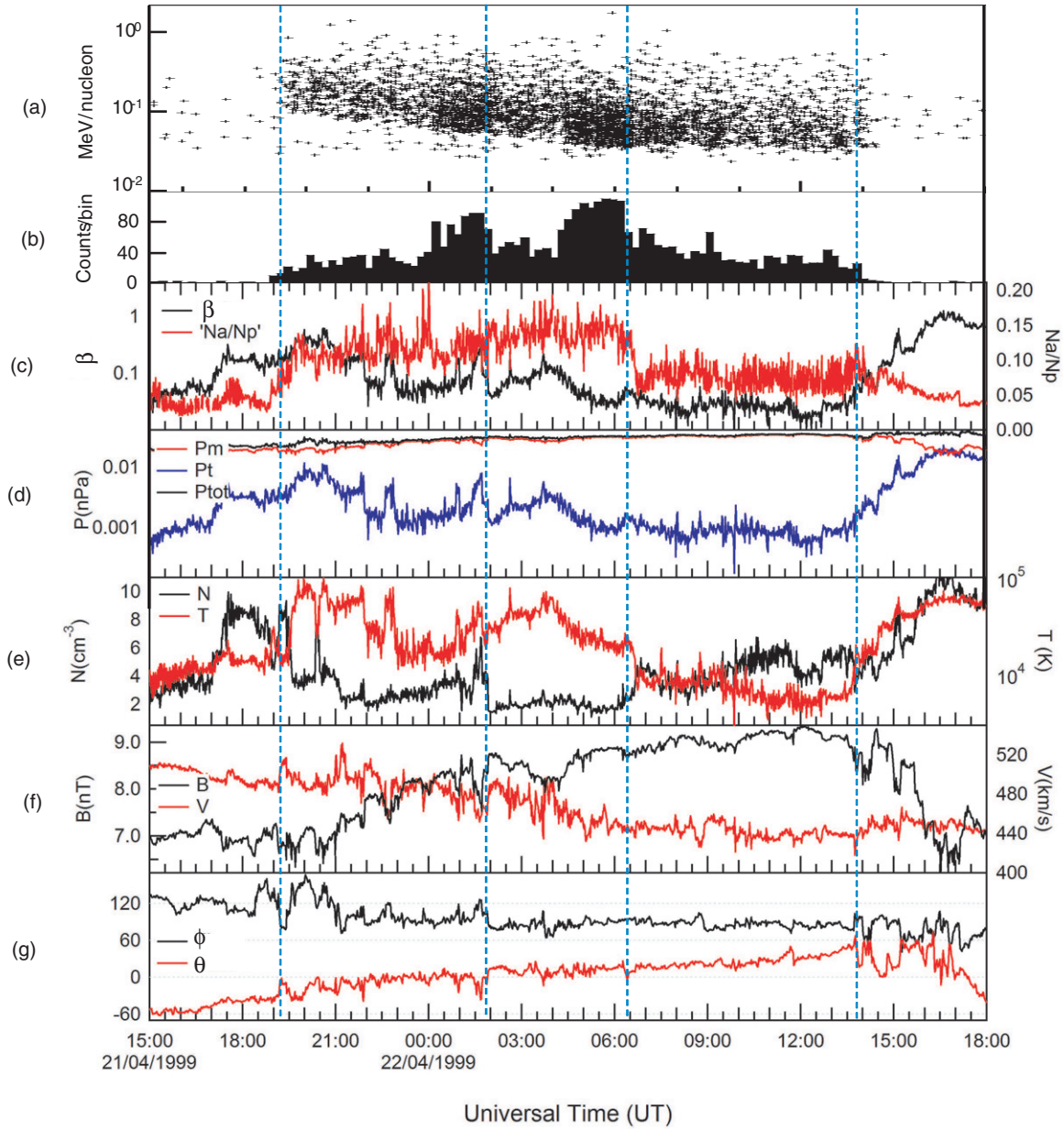

Figure 2. Combined energetic ions and plasma–magnetic field parameters for the 1999 April 21–22 SEP event. In the first two panels, the energetic particle data with the same format as Figure 1 (adapted from Gosling et al. 2004) are repeated. (c) The ratio between plasma and magnetic pressures β and the α to proton density ratio, (d) kinetic, magnetic, and total pressures, (e) plasma density and temperature, (f) magnetic field magnitude and plasma speed, and (g) the polar angles of the magnetic field vector defined as $\varphi = \tan^{-1}(B_Y, B_X)$, $\theta = \tan^{-1}(B_Z/(B_X^2 + B_Y^2)^{0.5})$ in the range $[-180^\circ, +180^\circ]$ and $[-90^\circ, +90^\circ]$, respectively.

(A color version of this figure is available in the online journal.)

to region 3, with a gradual trend to increase during region 1 and a gradual decrease during region 3. This feature could be related to the SEP energy distribution at the flare where they are accelerated. In the following, it will be shown that these three regions, identified according to the SEP structure, are separated by magnetic helicity structures and are characterized by different plasma and magnetic field parameters.

Panels (c)–(f) in Figure 3 show the results of magnetic helicity analysis, with the same format as Figure 1. For this event the spectral index of magnetic helicity density spectrum, computed via a fast Fourier transform, is −2.52, and the compensated magnetic helicity reported in panel (c) has been obtained multiplying $H_m^r(k, t)$ by $f^{2.52}$. The strongest and statistically more reliable (see panels (d)–(f)) helicity structures seem to be related with the SEP modulation: intense helicity structures are observed in the first part of region 1, corresponding with the arrival of the most energetic SEP, and other helicity structures are detected at the boundaries of regions 2 and 3, while in the inner parts of these regions the values of magnetic helicity are very low.

The same event was analyzed by Mazur et al. (2000) and Gosling et al. (2004) but these authors could not find any obvious associations with changes in magnetic field orientation and/or plasma parameters. While we already showed that magnetic field does have some helicity signature in proximity of SEP modulation events, we will, in the following analysis, also show that some signatures can also be detected in plasma parameters. In Figure 4, the energetic particle data are repeated in the first two

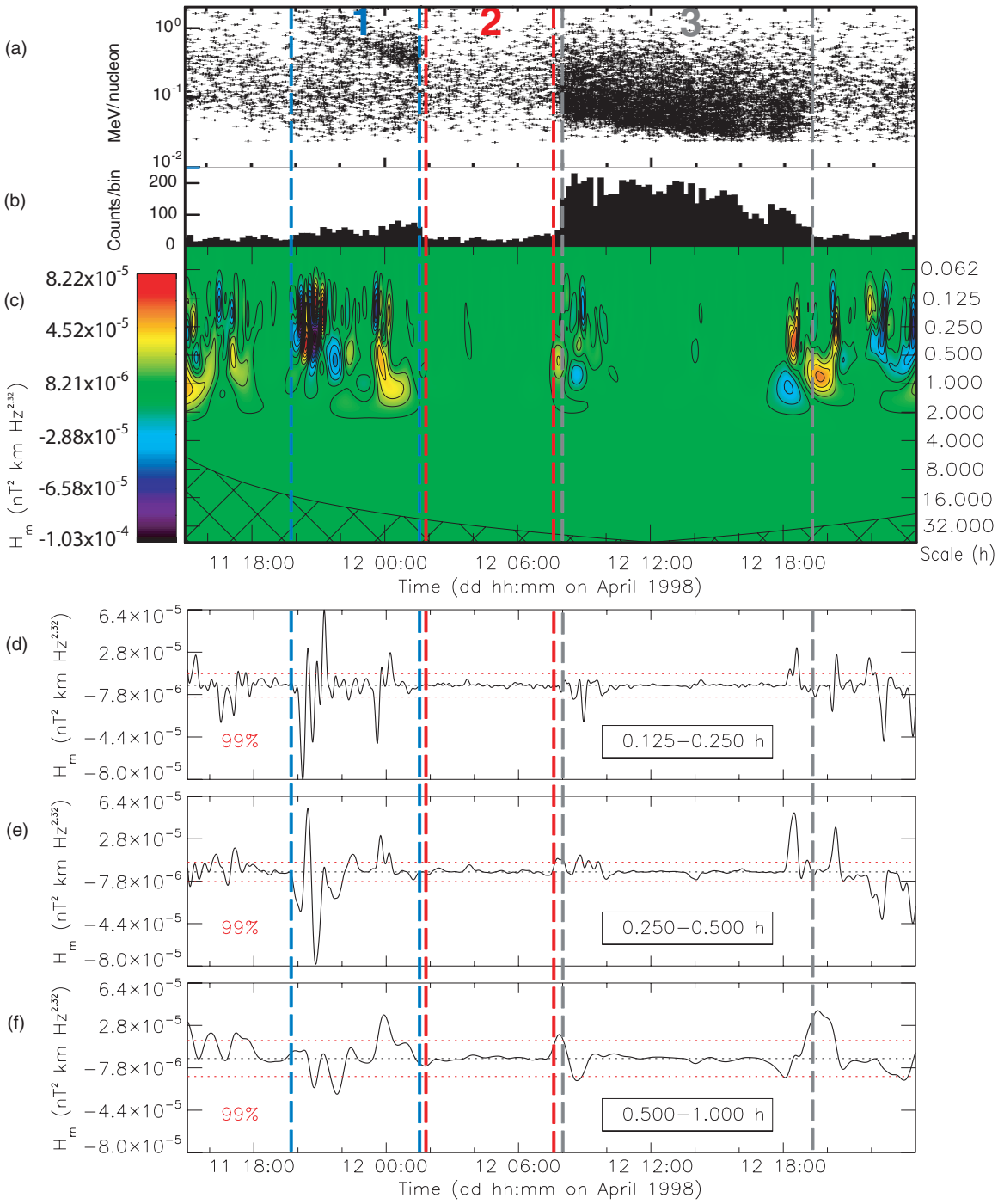

Figure 3. Combined energetic heavy ions (all species except H; adapted from Gosling et al. 2004) and magnetic helicity analysis for the 1998 April 11–12 SEP event. The format is the same as Figure 1.

(A color version of this figure is available in the online journal.)

panels and the plasma and magnetic field parameters (with the same format as Figure 2) are plotted in panels (c)–(g). In the next two panels (h) and (j), the plasma heavy-ion composition data measured by SWICS (Gloeckler et al. 1998) on board *ACE* are shown. Heavy-ion elemental abundances (X/H) and the oxygen and carbon charge state ratios are shown in panels (h) and (i), respectively.

It can be noted that the three regions corresponding to SEP structure, reported with the colored dashed lines, are characterized by different magnetic and plasma parameters. In region 2, the plasma β, the kinetic pressure, and the plasma temperature are lower with respect to their values measured in regions 1 and 3; the magnetic field orientation is stable, being $\phi \sim -77°, \theta \sim 4°$. Moreover, moving to region 3 the magnetic field magnitude decreases and the magnetic field orientation changes significantly, being $\phi \sim -37°, \theta \sim 37°$ in the inner part of region 3. The variation of these parameters occurs gradually, from 08:00 to 10:00 of April 12, i.e., in the time period when the helicity structures are observed. Similarly, the gradual increase of the magnetic field magnitude associated with the magnetic

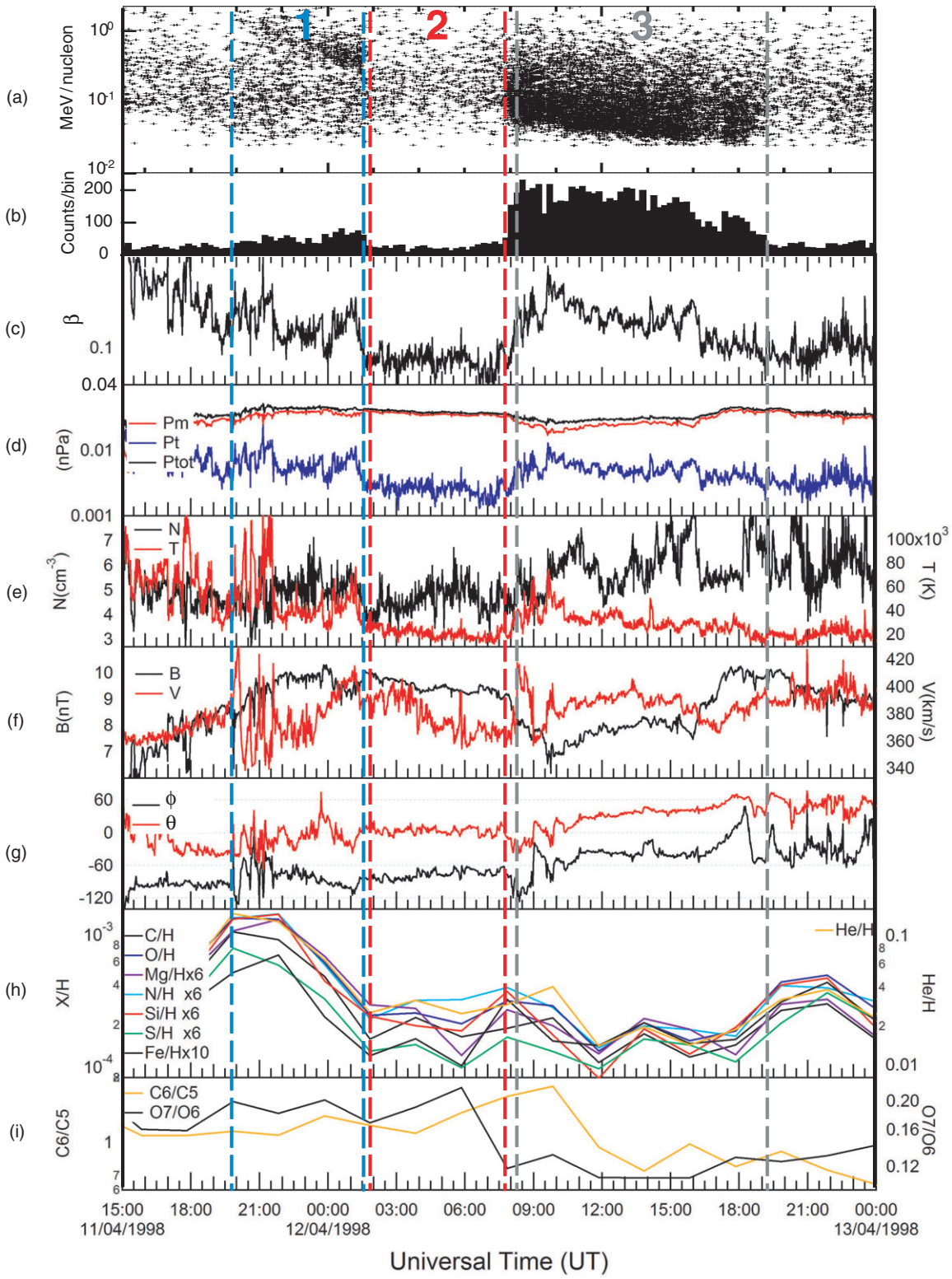

Figure 4. Combined energetic ions (all species except H; adapted from Gosling et al. 2004), plasma–magnetic field parameters, and plasma heavy-ion composition for the 1998 April 11–12 SEP event. The format is the same as Figure 2. In the last two panels, the heavy-ion elemental abundances (X/H) (panel (h)) and the oxygen and carbon charge state ratios (panel (j)) are shown, respectively.

(A color version of this figure is available in the online journal.)

field rotation observed after 16:00 of April 12 matches the helicity structures at the end of region 3. Therefore these helicity structures probably identify the boundaries of adjacent magnetic structures containing different plasmas. Moving from region 2 to region 1, the magnetic field orientation rotates while the magnetic field magnitude does not vary significantly.

As we already saw in the previous discussion, especially regions 2 and 3 seem to show different features in magnetic field

and plasma parameters that could suggest a different origin at the Sun. A further tool that we can use to corroborate this possibility is represented by minor ion observations.

As a matter of fact, heavy-ion elemental abundance and ionic charge state composition are useful tracers to identify different source regions at the Sun since, even though the kinetic properties of the streams experience dynamic interactions between slow and fast streams during the expansion, the elemental and charge composition remains unchanged in the heliosphere (Zurbuchen et al. 2000, and references therein). Moving from region 1 to region 2 in panel (h), all the heavy-ion abundances decrease; the further reduction of heavy-ion abundances observed at 10:00 followed by an increase after 18:00 of April 12 seems to be related to region 3. Moreover, the reduction of the relative concentration O7/O6 observed at 07:00 followed by the reduction of C6/C5 observed at 10:00 of April 12 is likely related to the passage from region 2 to region 3. These observations, although characterized by low time resolution (2 hr), suggest that these regions are originated at different sites on solar corona: region 3 comes from a coronal region with cooler electron temperature with respect to both regions 1 and 2 (Hundhausen et al. 1968; Owocki et al. 1983; Zhao et al. 2009) while regions 1 and 2 come from coronal regions with same temperature but different heavy-ion composition.

Therefore the combined set of plasma, magnetic, and composition observation suggests that regions 1, 2, and 3 correspond to adjacent structures originated at different sites on solar corona, with a nearly independent evolution from there. The different magnetic connectivity of these structures with the flare originating the SEP could explain the SEP modulations. In fact, regions 1 and 3 should be magnetically connected with the flare, while region 2, corresponding to the long SEP interruption, should not be connected.

It is interesting to note that the most intense helicity structures observed from 20:00 to 21:30 of April 11, associated with abrupt variations of plasma speed and temperature, seem to be produced by the arrival of the most energetic SEP. This observation could suggest the presence of some wave-particle instabilities as suggested by Ng & Reames (1994).

2.3. 2002 October 20–21 Event

In Figure 5, we show an SEP event recorded by *WIND* between 2002 October 20 and 21. The spectrogram in panel (a) shows the inverse of speed expressed in hr AU^{-1} and has been adapted from Chollet & Giacalone (2008).

According to the uniform distribution of particles in the spectrogram, this event has been considered as a clear example of an SEP event with no dropouts (Chollet & Giacalone 2008). This event starts approximately at 17:30 on October 20 with the arrival of the most energetic particles and shows a clear dispersion relation which suggests that the particles are accelerated impulsively at the Sun. Panels (c)–(f) show the results of magnetic helicity analysis with the same format as Figure 1. For this event the spectral index of magnetic helicity density spectrum, computed via a fast Fourier, is −2.34, and in panel (c) we report the compensated magnetic helicity scalogram obtained by multiplying $H_m^r(k,t)$ by $f^{2.34}$. During the entire SEP event, several helicity structures at different timescales are observed. However, according to the confidence analysis, none of these helicity fluctuations is significant at the three timescales examined, except for the one observed at 18:40 of October 20, which marks the beginning of the SEP event (panels (d)–(f)).

In Figure 6, the energetic particle data are repeated in the first panel and the plasma and magnetic field parameters, with the same format as Figure 2, are plotted in panels (c)–(g). At odds with previous SEP events discussed so far, plasma parameters do not show any noticeable change moving across the event. Large-scale behavior of these parameters looks pretty steady and only small-scale ($\ll$1 hr) fluctuations can be seen. The only parameters that show some activity are the two angles of the magnetic field θ and ϕ. This variability is mainly due to the presence of Alfvénic fluctuations (not shown), which act on the direction of the local magnetic field without changing its intensity. As a matter of fact, magnetic field intensity remains confined between 5 and 6 nT throughout the analyzed time interval.

The dominant presence of these fluctuations explains the low helicity level we showed in the previous panel since the nature of Alfvénic fluctuations is stochastic and clear helicity signatures can happen only by chance. Thus, in this particular event, magnetic field and plasma parameters show the homogeneity of this region, which is consistent with the absence of dropouts.

2.4. 1999 January 9–10 Event

The fourth SEP event that we illustrate is the one recorded by *ACE* during 1999 January 9–10 and shown in panels (a) and (b) of Figure 7 (Mazur et al. 2000; Gosling et al. 2004). Panels (a) and (b) have the same format as those in Figure 1 and are adapted from the online plots available at http://www.srl.caltech.edu/ACE/ASC/DATA/level3/uleis/.

The SEP event starts at about 14:00 on January 9 with the arrival of ions with energy of about 0.6 MeV $nucleon^{-1}$, finishes approximately at 05:30 on January 10 with the arrival of the last particles with energy of 0.02 MeV $nucleon^{-1}$, and shows a clear dispersion relation, which suggests that the particles are accelerated impulsively at the Sun. This event shows several SEP modulations where the counts change gradually over timescales of about an hour: the maximum counts are about 200 particles bin^{-1}, while the minimum counts are comparable with the background level observed before and after the SEP event.

Panels (d)–(f) show the results of magnetic helicity analysis with the same format as Figure 1. For this event the spectral index of magnetic helicity density spectrum, computed via a fast Fourier, is −2.46, and the compensated magnetic helicity reported in panel (c) has been obtained by multiplying $H_m^r(k,t)$ by $f^{2.46}$.

The scalogram in panel (c) shows that, during the SEP event, several helicity structures are observed. Most of them are statistically significant, as shown in panels (d)–(f), within each of the three ranges of scales. During this particular SEP event it is rather difficult to associate, in a clear way, the beginning or the end of a dropout event with corresponding magnetic helicity signatures. In particular, some of these helicity structures seem to be associated with higher SEP counts (for example at 01:00 of January 10). Moreover, within the interval from 22:00 of January 9 to 02:00 of January 10, the helicity behavior seems to be very complicated, showing simultaneous structures at different timescales. There is no doubt that this event is by far the most complicated we have analyzed and our technique does not show the best performance, although it still shows clearly that we are dealing with a rather complex magnetic field topology, which, somehow, might be reflected in the multiple dropouts seen during this event.

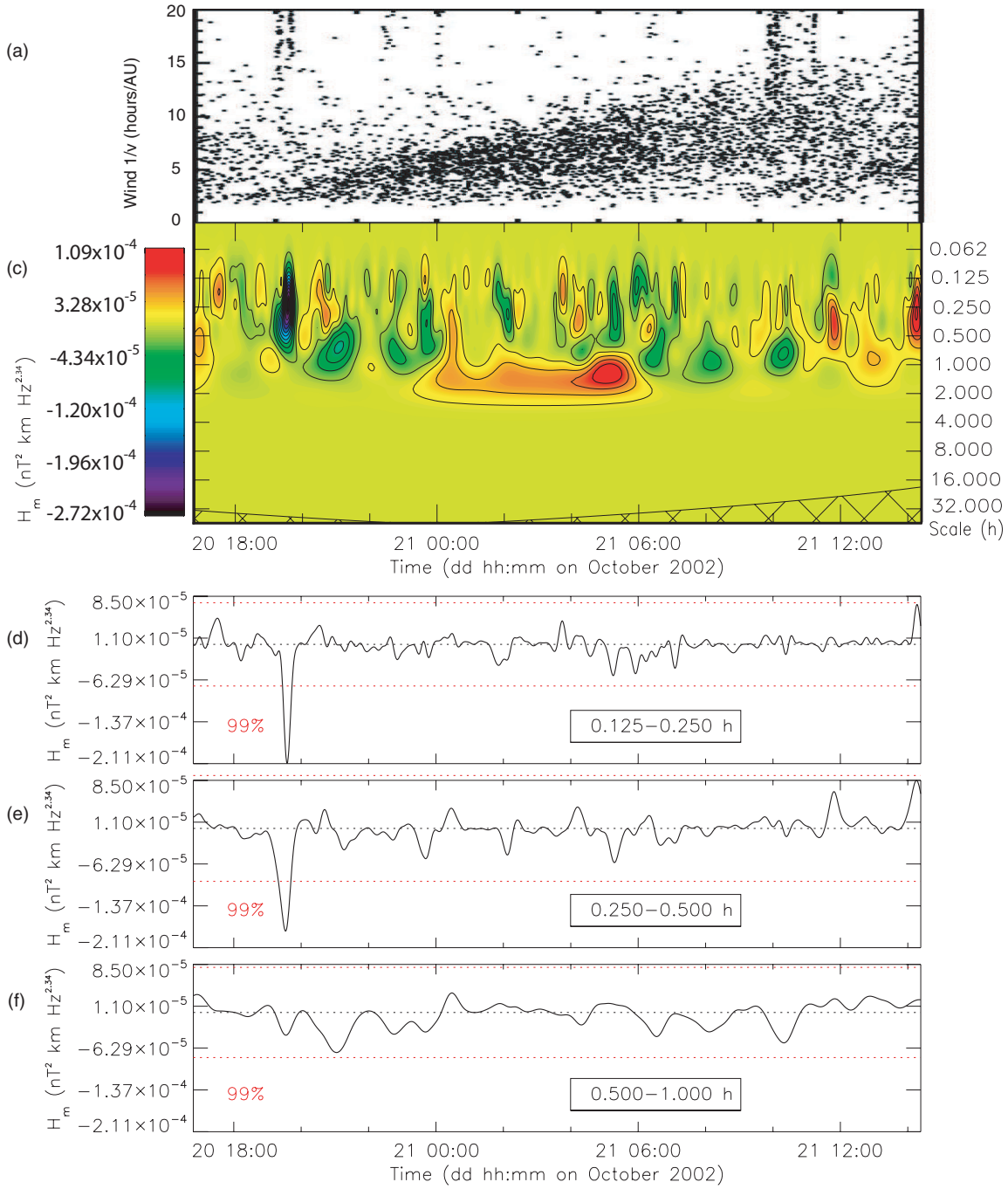

Figure 5. Combined energetic ions (all species except H; adapted from Gosling et al. 2004) and magnetic helicity analysis for the 2002 October 20–21 SEP event. (a) The inverse of speed of energetic ions, expressed in hr AU^{-1}, vs. their arrival time (adapted from Chollet & Giacalone 2008). (c)–(f) The results of magnetic helicity analysis with the same format as Figure 1.

(A color version of this figure is available in the online journal.)

In Figure 8, the plasma and magnetic field parameters with the same format as Figure 2 are shown. During this SEP event, magnetic field magnitude and plasma parameters clearly change on scales that are comparable to those on which SEP modulation is manifested; the plasma β shows several modulations (panel (c)) while the total pressure is approximately constant (panel (d)). In the four regions highlighted by the yellow shading, the plasma temperature is higher, the magnetic field magnitude is lower (such that the reduction in the magnetic pressure balances the increase in thermal pressure), and the plasma speed is rather constant and is different with respect to the speed of the surrounding plasma. These characteristics suggest that the plasma in this region is dominated by pressure-balanced structures (PBSs). In the PBS observed at 22:30 on January 9, the magnetic field magnitude decreases to less than 1 nT (not shown) and the magnetic pressure is negligible. In the other three PBSs, the magnetic field magnitude is only 20% lower than the external field, and the thermal and magnetic pressures are comparable.

The SEP counts are lower within these PBSs, but higher within low plasma β regions. The scatter plot in Figure 9 reports, in logarithmic scales, the SEP counts as a function of the plasma

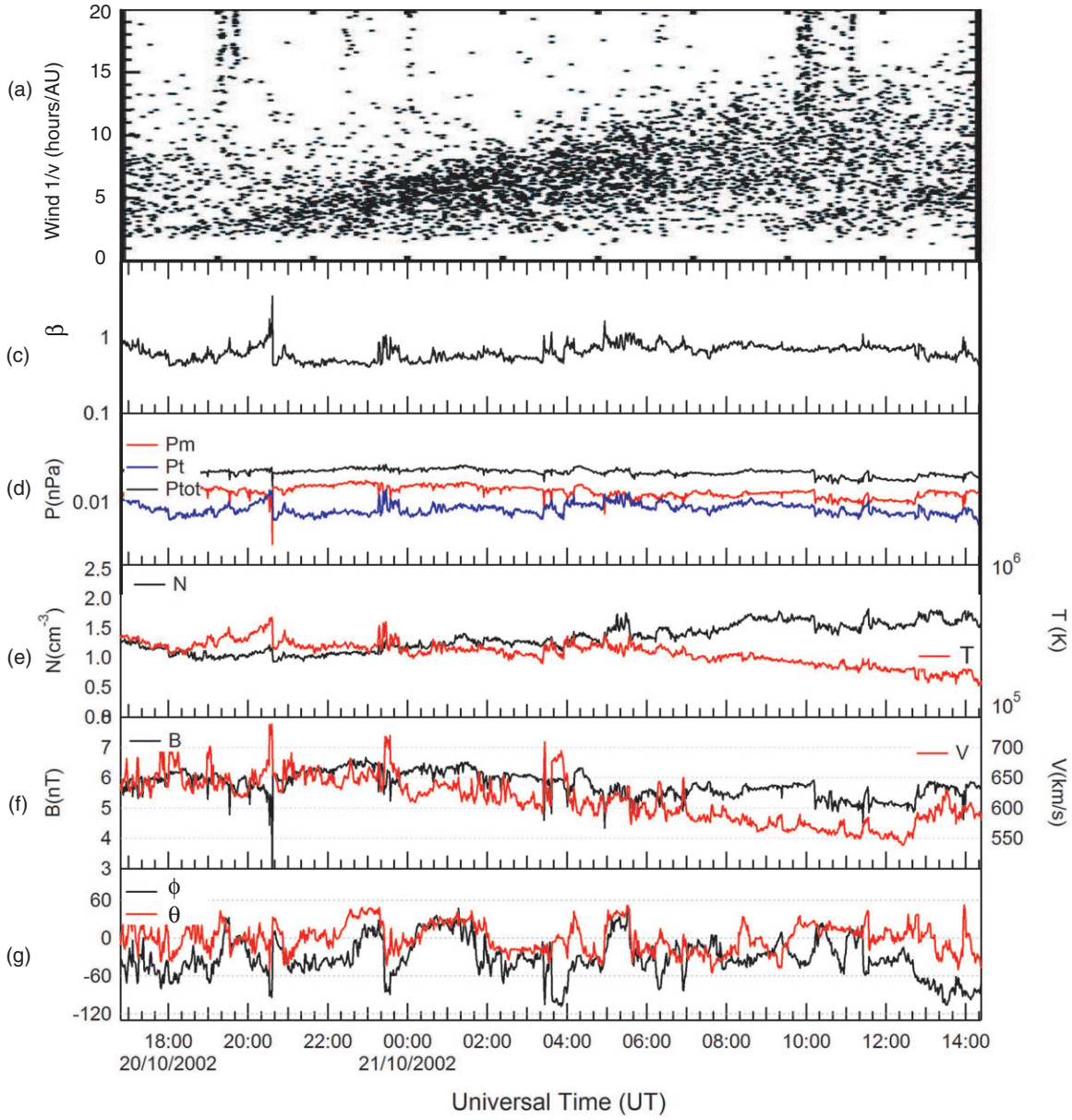

Figure 6. Combined energetic ions and plasma–magnetic field parameters for the 2002 October 20–21 SEP event. The energetic particle data are repeated in the first panel (adapted from Chollet & Giacalone 2008) and the format is the same as Figure 2.

(A color version of this figure is available in the online journal.)

β measured during the SEP event (from 16:00 of January 9 to 07:00 of January 10). The points measured within the PBS observed at 22:30 on January 9 are not included in this plot since here the β is two orders of magnitude higher. The black line is the best linear fit through the distribution of the log of count values versus the log of β values and *corr* is the relative correlation coefficient that shows a certain degree of negative correlation between integrated SEP counts and plasma β values.

3. SUMMARY AND CONCLUSIONS

In this paper, we performed a detailed analysis of the local magnetic field and plasma parameters measured during impulsive SEP events in order to check the possibility to highlight some signature of SEP dispersionless modulations, also called SEP dropout events, in the solar wind parameters.

We provide the first direct observational evidence for an interpretation of dropouts in terms of magnetic connection to solar sources of particles and solar wind plasma. As a matter of fact, so far there has been no mention of any clear evidence of an association between these dropout events and local changes in the magnetic field or plasma parameters in the literature (Mazur et al. 2000; Gosling et al. 2004; Chollet & Giacalone 2008).

Various models related these dropouts to abrupt changes of magnetic connectivity of the observing spacecraft with the flare site at the Sun. The variations of magnetic connectivity with the flare could be due to both the field-line footpoint motion at the photosphere (Mazur et al. 2000) and the random walk of field lines in the solar wind (Giacalone et al. 2000). Other models related these changes of magnetic connectivity to the different characteristics of turbulence in the solar wind (Ruffolo et al. 2003 and Pommois et al. 2005). Alternatively, without changing the magnetic connection with the flare, these dropouts

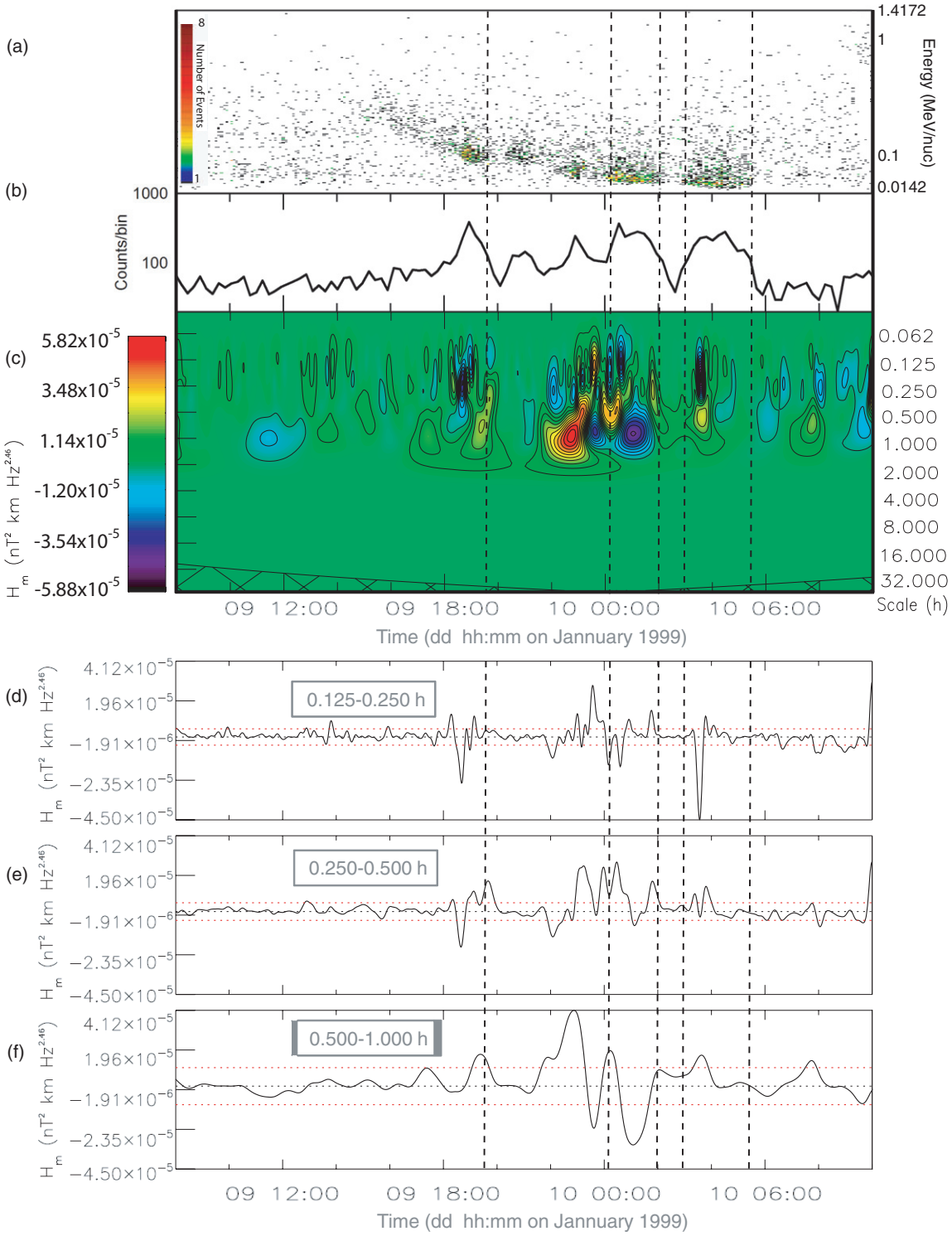

Figure 7. Combined energetic ions (adapted from online plots available at http://www.srl.caltech.edu/ACE/ASC/DATA/level3/uleis/) and magnetic helicity analysis for the 1999 January 9–10 SEP event. The format is the same as Figure 1.

(A color version of this figure is available in the online journal.)

could be a consequence of scattering due to the intermittency in the solar wind turbulence (Kaghashvili et al. 2006). Although these models do not explicitly require any local signatures in the plasma or magnetic field data, we found that, frequently, local signatures associated with these SEP dropouts are observed.

In particular, the study of local magnetic field topology by means of magnetic helicity allowed us to identify magnetic boundaries, associated with variations of plasma parameters, which are thought to represent the borders between adjacent magnetic flux tubes (Bruno et al. 2001; Li 2007; Borovsky 2008). While many or most dropouts are associated with these boundaries, not all dropout features have clear magnetic or plasma signatures. However, it should be noted that the flux tubes may have, sometimes, ill-defined boundaries (Seripienlert

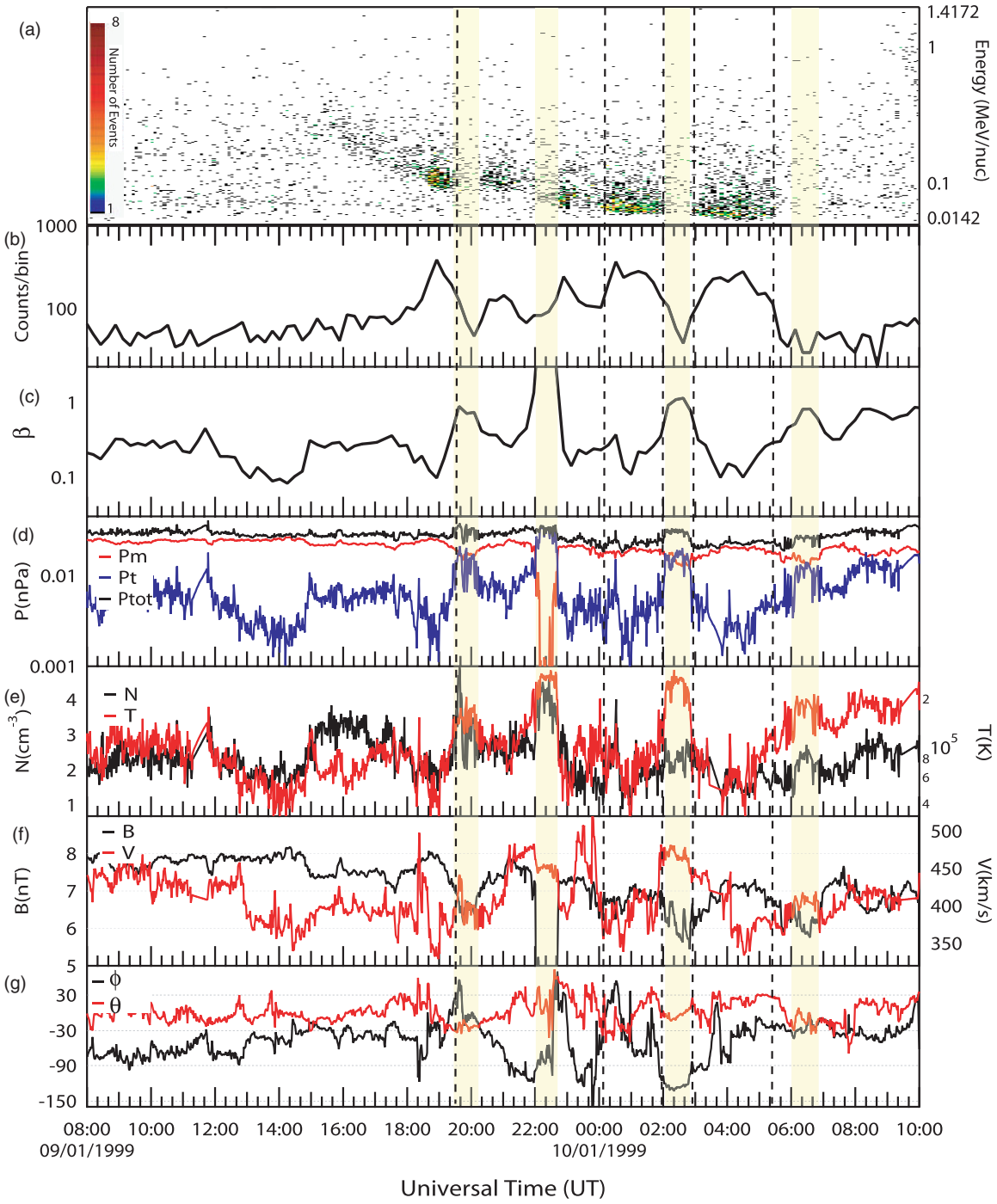

Figure 8. Combined energetic ions (adapted from online plots available at http://www.srl.caltech.edu/ACE/ASC/DATA/level3/uleis/) and plasma–magnetic field parameters for the 1999 January 9–10 SEP event. The format is the same as Figure 2.

(A color version of this figure is available in the online journal.)

et al. 2010). Anyhow, we found convincing evidence for an association of these magnetic helicity signatures with borders of impulsive SEP events or with SEP dropout events.

For example, the SEP event of 1999 April 21–22 is characterized by a dispersionless onset and a dispersionless end, which are both associated with such magnetic boundaries. In this event, the SEPs are detected within a CME and the end of SEPs is observed when the spacecraft exits from this CME. Conversely, the magnetic boundary corresponding to the onset of the SEP is located inside the CME and could be related to the inner CME structure. Therefore, the magnetic field lines of the CME along which SEPs are propagating can be considered as a flux tube connected with the Sun at the flare sites. This implies that at least this portion of the CME field lines remains rooted at the Sun as suggested by the possible counterstreaming electron signature found by Gosling et al. (2004) for this same event.

On the other hand, event on 1998 April 11–12 is a clear example of an SEP dropout: a long-lasting interruption (6 hr) of SEP, with dispersionless margins, occurs approximately in the middle of the event whose total duration is 22 hr. It is

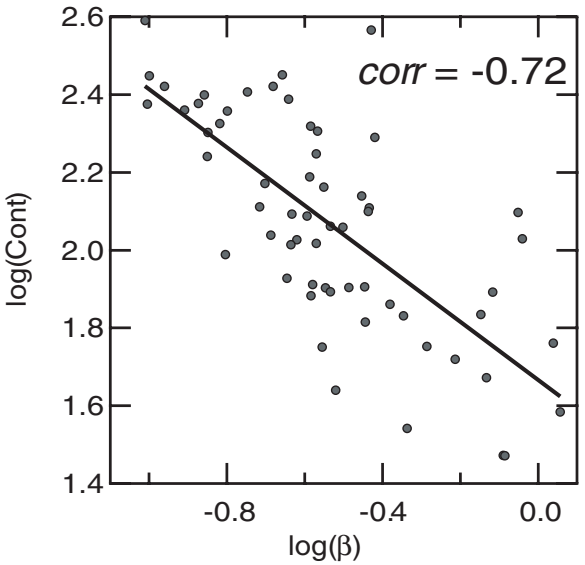

Figure 9. SEP counts as a function of the plasma β, in logarithmic scales, measured during the 1999 January 9–10 SEP event (from 16:00 of January 9 to 07:00 of January 10). The points measured within the PBS at 22:30 on January 9 are not included in this plot. The black line is the best linear fit through the distribution of the log of count values vs. the log of β values, and *corr* is the relative correlation coefficient. A certain degree of negative correlation between integrated SEP counts and plasma beta values is observed.

found that the three regions—at the beginning of the event with higher energy SEPs, the central region with the dropout, and the last one with lower energy SEPs—are characterized by different plasma and magnetic field parameters. Moreover, these regions are separated by the magnetic boundaries identified by our magnetic helicity technique and also have different heavy-ion compositions. These observations support the idea that these regions correspond to three magnetic flux tubes, containing plasmas originated at different sites on solar corona. Since the SEP void matches the central flux tube, we can infer that, when the SEPs are accelerated, this flux tube was not connected with the flare site. In this case, without invoking the footpoint motion, we could infer that the flare occurs in a region of the solar corona not connected with this flux tube, but connected with the two other flux tubes filled with SEPs. However, the quasi-radial expansion of the wind suggests that these flux tubes originated at neighboring regions at the Sun, not too far apart from each other.

The 2002 October 20–21 event strongly supports the general idea that dropouts are related to the passage through different magnetic flux tubes. Indeed, during the entire event the SEP are continuously detected, and, accordingly, nor magnetic boundaries neither variations of plasma parameters indicating the passage through adjacent flux tubes are observed.

Much more complex is the event of 1999 January 9–10, where dropout borders cannot be generally associated with magnetic helicity signatures. These dropouts, which are more gradual and have shorter time duration (1 hr), seem to be associated with PBSs characterized by higher plasma temperature and lower magnetic field magnitude with respect to the surrounding plasma. In one of these PBS the magnetic field intensity decreases to less than 1 nT while in the others the magnetic field magnitude is only 20% lower than the external field.

Isolated structures with a significant decrease in magnetic field intensity are frequently observed in the solar wind and are called magnetic holes (Turner et al. 1977). While the first studies concentrated on small-scale magnetic holes (tens of seconds), more recently it has been demonstrated that these magnetic holes are PBSs with similar properties at different scales and with the full range of decrease in magnetic field intensity relative to the ambient field (Stevens & Kasper 2007). Therefore, the observed PBSs could possibly be considered as large-scale magnetic holes.

Stevens & Kasper (2007) suggested that these magnetic holes are generated as a consequence of magnetic mirror instability near the solar corona and then they are passively advected by the solar wind. However, it seems that the magnetic holes generated with this mechanism are not magnetically isolated from the plasma environment (Horbury & Lucek 2009), and therefore they are incapable of shielding the SEP.

A different origin for magnetic holes is based on magnetic reconnection in the high solar corona of closed magnetic loops with open magnetic field lines (Zurbuchen et al. 2001). The reconnection process locally increases the plasma temperature, and then the further acceleration, driven by magnetic tension, increases the plasma density. During the convection, the evolution toward a pressure balance configuration causes the magnetic field depletion. It is important to note that in this model the reconnection process could change the magnetic connection of these holes with the Sun. Therefore, these holes, which could be magnetically isolated from the plasma environment, could explain the observed particle dropouts.

This work was partially supported by the Agenzia Spaziale Italiana, contract ASI/INAF I/013/12/0. T.H.Z. and M.W. were supported in part by NASA contracts NNX08AI11G, NNX10AQ61G, NNX08AM64G and 44A-1085637.

APPENDIX

THEORETICAL SIGNIFICANCE LEVEL FOR THE REDUCED MAGNETIC HELICITY WAVELET SPECTRUM

To determine the significance levels for the reduced magnetic helicity wavelet spectrum one first needs to choose an appropriate background spectrum. It is then assumed that different realizations of the physical process (namely, the inference of high-amplitude signals in the magnetic helicity wavelet spectrum in coincidence with the SEP modulation) will be randomly distributed about this mean or expected background, and the actual spectrum can be compared against this random distribution. This spectrum is indeed used to establish a null hypothesis for the significance of a peak in the reduced magnetic helicity wavelet spectrum.

The background spectrum for the magnetic helicity can be obtained from the observed data by destroying the possible phase correlations existing between the y- and z-components of the magnetic field. In this way, we can build a magnetic helicity wavelet spectrum randomly fluctuating around zero helicity. In order to do so, both B_y and B_z are Fourier transformed and the relative phases randomized between $-\pi$ and π. Real and imaginary parts of B_y and B_z are then anti-transformed in order to obtain the relative uncorrelated time series. This procedure, obviously, does not change the total power and the spectral index of B_y and B_z. However, while peaks in the reduced magnetic helicity wavelet spectrum inferred from the observed data might be due to correlated rotations of the magnetic field components, those exhibited in the wavelet spectrum obtained from the uncorrelated data are certainly due to Gaussian random

noise. Hence, by comparing the local spectra of the reduced magnetic helicity with the (mean) background wavelet spectrum averaged in time over the whole observation period, it is possible to identify the magnetic helicity peaks above the expected background spectrum.

The null hypothesis for the reduced magnetic helicity wavelet spectrum is defined as follows. It is assumed that the mean background spectrum is given by the time-averaged (say global) of the magnetic helicity wavelet spectrum obtained from the uncorrelated B_y and B_z time series. If a peak in the magnetic helicity wavelet spectrum is significantly above this background spectrum, then it can be assumed to be a true feature with a certain confidence level. In this study we used a significance level of 1%, which is equivalent to "the 99% confidence level" and implies a test against the background level. The wavelet spectrum of a normally distributed random variable, representing a Gaussian physical process, is chi-square distributed with two degrees of freedom, denoted by χ_2^2 (Jenkins & Watts 1968). To determine the 99% confidence level for the reduced magnetic helicity spectrum, one multiplies the background spectrum by the 99th percentile value for χ_2^2 (Gilman et al. 1963).

The results of the confidence level analysis are shown in panels (d)–(f) of Figures 1, 3, 5, and 7. Here the continuous black lines show the scale-averaged reduced magnetic helicity within the frequency range indicated in each panel while the dotted red lines show the 99% confidence levels. Whenever a peak in the scale-averaged magnetic helicity is above the red lines it means that there is only a 1% probability that we obtained this result by mere chance.

REFERENCES

Borovsky, J. E. 2008, JGRA, 113, 8110
Bruno, R., Carbone, V., Veltri, P., Pietropaolo, E., & Bavassano, B. 2001, P&SS, 49, 1201
Bruno, R., & Dobrowolny, M. 1986, AnGeo, 4, 17
Bruno, R., Pietropaolo, E., Servidio, S., et al. 2008, AGUFM, 42, A6
Chollet, E. E., & Giacalone, J. 2008, ApJ, 688, 1368
Giacalone, J., Jokipii, J. R., & Mazur, J. E. 2000, ApJL, 532, L75
Gilman, D. L., Fuglister, F. J., & Mitchell, J. M., Jr. 1963, JAtS, 20, 182
Gloeckler, G., Cain, J., Ipavich, F. M., et al. 1998, SSRv, 86, 497
Gosling, J. T., Skoug, R. M., McComas, D. J., & Mazur, J. E. 2004, ApJ, 614, 412
Kaghashvili, E. Kh., Zank, G. P., & Webb, G. M. 2006, ApJ, 636, 1145
He, J., Marsch, E., Tu, C., Yao, S., & Tian, H. 2011, ApJ, 731, 85
Horbury, T. S., & Lucek, E. A. 2009, JGRA, 114, 5217
Hundhausen, A. J., Gilbert, H. E., & Bame, S. J. 1968, JGR, 73, 5485
Jenkins, G. M., & Watts, D. G. 1968, Spectral Analysis and Its Applications (London: Holden-Day),
Lepping, R. P., Acũna, M. H., Burlaga, L. F., et al. 1995, SSRv, 71, 207
Li, G. 2007, in AIP Conf. Proc. 932, Turbulence and Nonlinear Processes in Astrophysical Plasmas, ed. D. Shaikh & G. P. Zank (Melville, NY: AIP), 26
Li, G. 2008, ApJL, 672, L65
Lin, R. P., Anderson, K. A., Ashford, S., et al. 1995, SSRv, 71, 125
Mason, G. M., Gold, R. E., Krimigis, S. M., et al. 1998, SSRv, 86, 409
Matthaeus, W. H., & Goldstein, M. L. 1982, JGR, 87, 6011
Matthaeus, W. H., Goldstein, M. L., & Roberts, D. A. 1990, JGR, 95, 20673
Mazur, J. E., Mason, G. M., Dwyer, J. R., et al. 2000, ApJL, 532, L79
McComas, D. J., Bame, S. J., Barker, P., et al. 1998, SSRv, 86, 563
Miller, J. A., & Vinas, A. F. 1993, ApJ, 412, 386
Neugebauer, M., & Goldstein, R. 1997, in Coronal Mass Ejections, ed. N. Crooker, J. Joselyn, & A. Feynman (Washington, DC: AGU), 245
Ng, C. K., & Reames, D. V. 1994, ApJ, 424, 1032
Owocki, S. P., Holzer, T. E., & Hundhausen, A. J. 1983, ApJ, 275, 354
Podesta, J. J., & Gary, S. P. 2011, ApJ, 734, 15
Pommois, P., Zimbardo, G., & Veltri, P. 2005, AdSpR, 35, 647
Reames, D. V. 1999, SSRv, 90, 413
Ruffolo, D., Matthaeus, W. H., & Chuychai, P. 2003, ApJL, 597, L169
Seripienlert, A., Ruffolo, D., Matthaeus, W. H., & Chuychai, P. 2010, ApJ, 711, 980
Smith, C. W., L'Heureux, J., Ness, N. F., et al. 1998, SSRv, 86, 613
Stevens, M. L., & Kasper, J. C. 2007, JGRA, 112, 5109
Telloni, D., Bruno, R., D'Amicis, R., Pietropaolo, E., & Carbone, V. 2012, ApJ, 751, 19
Torrence, C., & Compo, G. P. 1998, BAMS, 79, 61
Turner, J. M., Burlaga, L. F., Ness, N. F., & Lemaire, J. F. 1977, JGR, 82, 1921
von Rosenvinge, T. T., Barbier, L. M., Karsch, J., et al. 1995, SSRv, 71, 155
Zhao, L., Zurbuchen, T. H., & Fisk, L. A. 2009, GeoRL, 36, L14104
Zurbuchen, T. H., Hefti, S., Fisk, L. A., Gloeckler, G., & Schwadron, N. A. 2000, JGR, 105, 18327
Zurbuchen, T. H., Hefti, S., Fisk, L. A., et al. 2001, JGR, 106, 16001
Zurbuchen, T. H., & Richardson, I. G. 2006, SSRv, 123, 31